Volume 12 | Number 25 | 7 July 2014 | Pages 4267–4532

Organic & Biomolecular Chemistry

www.rsc.org/obc

ISSN 1477-0520

ROYAL SOCIETY OF CHEMISTRY

PAPER

Isabelle Leray *et al.*

Aggregation-induced emission enhancement upon Al^{3+} complexation with a tetrasulfonated calix[4]bisazacrown fluorescent molecular sensor

Organic & Biomolecular Chemistry

PAPER

Aggregation-induced emission enhancement upon Al^{3+} complexation with a tetrasulfonated calix[4]bisazacrown fluorescent molecular sensor†

Cite this: *Org. Biomol. Chem.*, 2014, **12**, 4335

Yi-Bin Ruan, Alexis Depauw and Isabelle Leray*

Received 24th January 2014,
Accepted 26th March 2014

DOI: 10.1039/c4ob00187g

www.rsc.org/obc

Aggregation-induced emission and aggregation-induced emission enhancement have attracted much attention due to their great potential in real-world applications. Up to now most of the reports are based on the restriction of free rotation of the luminogens in the aggregates. In the present work, we found that the dansyl fluorophore with typical intramolecular charge transfer characteristic also exhibited aggregation-induced emission enhancement, which was based on the change of micro-environmental polarity of the fluorophore. In the light of the phenomenon, a new water-soluble ligand bearing a tetrasulfonated calix[4]arene was constructed for ratiometric detection of Al^{3+} based on an aggregation-induced emission enhancement mechanism. It displayed a distinct selectivity to Al^{3+} among the tested cations in lutidine buffer solution (pH 6–7) with a detection limit of 1.8 μM. A reversible response was also demonstrated by the addition of EDTA or F^-.

Introduction

Most fluorophores with planar and rigid aromatic structures, such as pyrene or perylene moieties, at high concentrations or in the solid state are usually weakly luminescent, which is considered to be associated with the formation of excimer/exiplex or aggregates.[1] Not until recently were aggregation-induced emission (AIE) and aggregation-induced emission enhancement (AIEE) phenomena discovered, demonstrating that upon formation of aggregates, emission efficiency is enhanced for some specific fluorophores.[2,3] These fluorophores share a common feature that they all have a rotatable single bond, which results in non-radiative decay of excitons. While in the aggregate state, restriction of free rotation in the free ligand opens up the radiative decay. Since this discovery, AIE/AIEE has been widely explored in various fields, especially as optical sensor materials. However, it should be noted that in the aggregate state, not only free rotation is suppressed, but also some factors like polarity are also quite different from that of the monomers in solution, which sometimes may strongly influence the optical properties, especially for fluorophores with intramolecular charge transfer (ICT). This means that it is possible to envisage molecules with rigid planar structure to have an AIE/AIEE effect. This can open up a new possibility to extend the structural diversity of luminogens with an AIE/AIEE effect. The danysl fluorophore is an attractive signalling reporting unit owing to its high sensitivity to the surrounding polarity.[4] Generally, with increasing polarity, it shows a red shift of its emission spectrum, and some specific interaction such as hydrogen bonding can lead to an increase of non-radiative decay.[5] In the present work, we intend to use this fluorophore to investigate the polarity-induced AIE/AIEE effect.

Aluminum is the most abundant metallic element in the Earth's crust. Due to its good physical and chemical properties, aluminum has been widely used in our daily life and thus health concerns of aluminum are considerably important. Exposure to a high dose of Al^{3+} can lead to neurotoxicity and deposits in the bone and the central nervous system.[6–8] For example, it is considered that Alzheimer's disease is strongly associated with the accumulation of Al^{3+} in the human body.[9] Conventional methods such as atomic absorption spectrometry and inductively coupled plasma atomic emission spectroscopy have been utilized to detect elemental aluminum and study its biological and environmental impact. However, they usually require expensive instruments and complicated sample preparation, making them unsuitable for on-site detection. Developing low cost and real-time monitoring systems is thus highly desirable. Fluorescent chemosensors have been well developed for the detection of important analytes in biological and environmental samples.[10–12] They exhibit several advantages over conventional methods, such as the low cost, easy sample preparation, on-site detection and biological imaging applications *in vivo*/*in vitro* samples. In this

PPSM, (UMR8531) Institut d'Alembert, ENS Cachan, CNRS, 61 av President Wilson, F-94230 Cachan, France. E-mail: Isabelle.LERAY@ppsm.ens-cachan.fr

†Electronic supplementary information (ESI) available: Some related spectroscopic data and NMR spectra of ligands **2** and **3**. See DOI: 10.1039/c4ob00187g

context, several typical binding motifs have been coupled with different chromophores/fluorophores for the detection of Al^{3+}, such as salicylic-Schiff base,[13–17] salicylic-amino base[18–20] and triazole.[21–23] To the best of our knowledge, these approaches were carried out in solutions containing various organic solvents. And up to now, scarce examples have been reported for the detection of Al^{3+} based on the AIE mechanism. An organic ligand consisting of triphenyl pyrrole was found to exhibit the AIE phenomenon in the presence of Al^{3+} in THF–H_2O mixtures (v/v = 25/75).[24] Besides the high fraction of organic solvent, it suffered from the interference of Pb^{2+} and Zn^{2+}. To deal with this problem, a water-soluble ligand has to be designed and synthesized first. Sulfonation is an efficient way to improve the water solubility of chromophores. Furthermore, investigations on the interaction of a surfactant containing sulfonate with Al^{3+} have shown that the strong electrostatic interaction could lead to precipitation of the complex. Their results indicated that the competition among sulfonate monomers, micelles and hydroxyl ions for Al species controls the behavior of the system.[25] Therefore the sulfonate group is considered an ideal choice in our present work to deal with water solubility and binding affinity with Al^{3+}. For continuous work on the attempt at developing fluorescent chemosensors based on the framework of calix[4]arene,[26–29] we envisage to introduce the sulfonate groups into the calix[4]arene moiety bearing dansyl as the fluorophore and investigate the interaction between the sulfonate group and Al^{3+} in a fluorometric manner.

Results and discussion

The synthesis of compound **3** was accomplished according to the procedure displayed in Scheme 1, starting from the tetratosylate **1**.[30] Dansylamide was reacted with 0.5 equiv. tetratosylate **1** in the presence of K_2CO_3 in the refluxing MeCN overnight. The crude product was isolated by column chromatography to afford **2** in 47% yield. **3** was obtained by direct sulfonation of **2** with chlorosulfonic acid, followed by neutralization with $NaHCO_3$ in pyridine–H_2O mixed solution in 54% yield. **3** was well characterized by ^1H, ^{13}C NMR and HRMS spectra. The 1,3-alternate conformation of **3** was deduced from the singlet peak (8H) of $ArCH_2Ar$ at 3.90 ppm in D_2O (Fig. S1†).

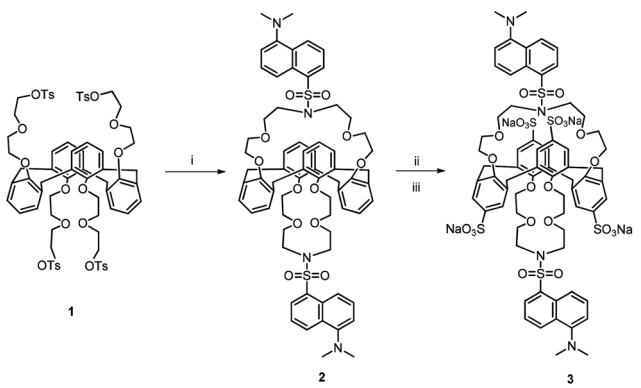

Scheme 1 Synthetic routine of **3**, (i) dansylamide–K_2CO_3–MeCN, reflux overnight, 47%; (ii) HSO_3Cl–CH_2Cl_2, –10 °C to RT; (iii) H_2O–pyridine–$NaHCO_3$, RT, 54%.

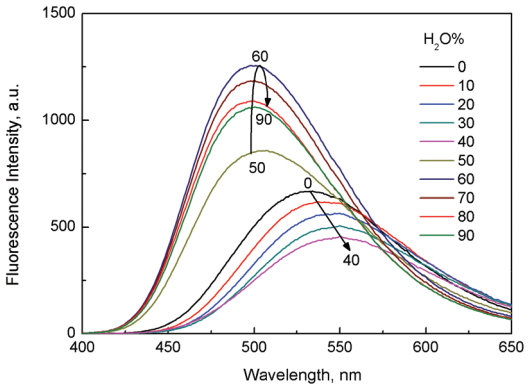

Fig. 1 Fluorescence spectra of **2** in EtOH–H_2O mixed solution with different volumetric fractions of H_2O; [**2**] = 10 μM, λ_{ex} = 338 nm.

Photophysical behavior of **2** was investigated in EtOH–H_2O mixed solution with different volumetric fractions of H_2O, as shown in Fig. 1. It is quite surprising to find that **2** exhibits an AIEE effect in EtOH–H_2O mixed solution. With increasing the water fraction to 40%, progressive fluorescence quenching with a red shift from 532 nm to 550 nm is observed. This is usually explained by the increase of solvent polarity with increasing water fraction, which can stabilize the charge separated state in the excited state and consequently lead to a red shift of the fluorescence spectra. In contrast, when the fraction of H_2O exceeds 40%, a level-off tail absorption band is observed and corresponding emission spectra display a remarkable blue shift from 550 to 500 nm and a fluorescence enhancement (about 2.7 fold when the water fraction is 0.6 compared with 0.4). This is in contrast to our expectation that increasing the polarity would induce the red shift of the ICT band. As we know that **2** is not soluble in H_2O, increasing the water fraction could lead to the formation of aggregates or small particles, which can be deduced from the level-off tail absorption. Fluorescence quenching is generally observed during the aggregation mainly because of the formation of H-aggregate. However, it is quite different in our case. This can be attributed to the dramatically reduced micro-environmental polarity of the dansyl fluorophore in the aggregated state, which may increase the radiative efficiency, and meanwhile the bulk steric effect caused by the calix[4]arene moiety prevented the compact stacking between the dansyl fluorophores. When the water fraction exceeds 60%, the fluorescence intensity is slightly quenched without a wavelength shift, indicating that precipitation of ligands from the solution started occurring. Therefore here we can conclude that formation of stable aggregates of **2** in H_2O can increase the fluorescence efficiency. This phenomenon can be utilized as a new fluorescent sensing approach based on analyte-induced formation of aggregates or

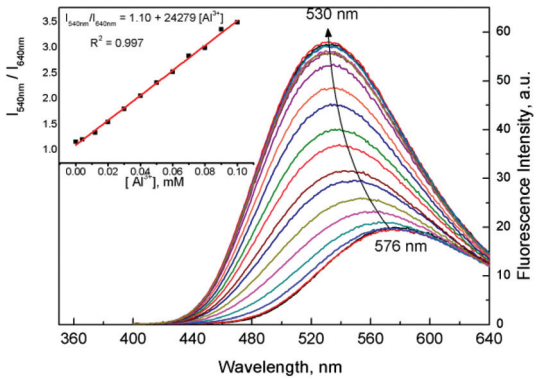

Fig. 2 Fluorescence spectra of **3** in the presence of increasing concentrations of Al^{3+} in lutidine buffer solution (pH = 6.0, 10 mM); inset: plot of ratiometric response I_{540}/I_{640} against Al^{3+} concentrations; [**3**] = 10 μM, λ_{ex} = 330 nm.

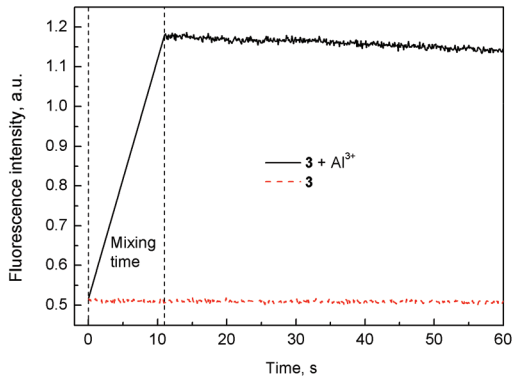

Fig. 3 Kinetic profile of **3** in the presence of Al^{3+} in lutidine buffer solution (pH = 6.0, 10 mM); fluorescence intensity was recorded at 540 nm; [**3**] = 10 μM, [Al^{3+}] = 25 μM, λ_{ex} = 328 nm.

small particles to construct a less polar micro-environment for ICT type fluorophores.

The pH-dependent absorption and emission spectra of **3** were recorded in H_2O. As shown in Fig. S3,† it exhibits a broad absorption band centered at 328 nm and an emission band at 579 nm under neutral and basic conditions, which can be attributed to intramolecular charge transfer from the dimethylamino group to the sulfonyl group. By decreasing the pH of the solution with the addition of $HClO_4$, the absorption band at 328 nm decreases and new peaks at 320 and 285 nm appear, which is characteristic of the dansyl fluorophore when its dimethylamino group is protonated. Meanwhile, a gradual decrease of the fluorescence intensity at 579 nm was observed. This can be attributed to the fact that protonation of the dimethylamino group blocks the intramolecular charge transfer. The pK_a of **3** in H_2O was obtained, by fitting from the titration, to be 4.7. At pH 6 (in lutidine buffer) **3** is weakly fluorescent with a quantum yield Φ_F of 3.8%, mainly because of high polarity and hydrogen bonding interaction between H_2O and the dansyl fluorophore rather than protonation of the dimethylamino group. The spectral response of **3** to Al^{3+} was then examined in lutidine buffer solution at pH 6.0. Fig. 2 displays evolution of the emission spectra of **3** upon Al^{3+} addition. When the concentration of Al^{3+} is lower than 0.1 mM, there is a gradual fluorescence enhancement and the emission band blue shifts from 576 nm to 530 nm. It reaches a plateau when the concentration is over 0.1 mM. Due to a 46 nm blue shift, it is possible for us to detect Al^{3+} by a ratiometric method. The ratio of fluorescence intensity at 540 and 640 nm as a function of the concentration of added Al^{3+} is plotted, as shown in Fig. 1 (inset). A nice linear dependence is obtained ranging from 0 to 0.1 mM. According to the $3\sigma/k$, the detection limit of our protocol was calculated to be 1.8 μM, meeting the requirement of WHO with a limit of 7.41 μM Al^{3+} in drinking water.[31] Beside this, the kinetics profile between **3** and Al^{3+} shows that the fluorescence intensity was enhanced immediately after addition of Al^{3+} without waiting time (Fig. 3). The reversibility between **3** and Al^{3+} was investigated in lutidine buffer solution

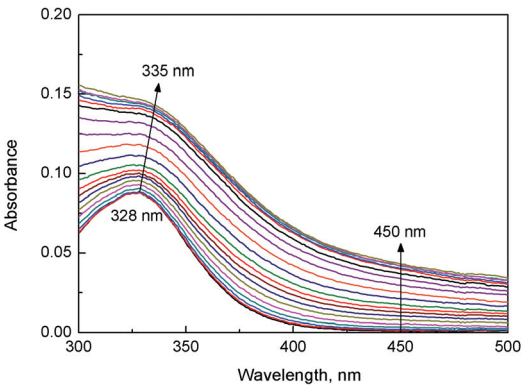

Fig. 4 Absorption of **3** in the presence of increasing concentrations of Al^{3+} in lutidine buffer solution (pH = 6.0, 10 mM); [**3**] = 10 μM.

at pH 6.0, as illustrated in Fig. S4.† With the addition of 2 equiv. of NaF or Na_2EDTA with respect to Al^{3+}, fluorescence spectra of **3** were recovered and nearly overlapped with free ligand. During the titration with Al^{3+} (Fig. 4), the absorption band of **3** at 328 nm shows a little red shift to 335 nm, which is quite close to that of **2** with neutral charge, probably indicating that partial negative charges were neutralized by Al^{3+}. Meanwhile, the level-off tail absorption band in the long wavelength region (450–500 nm) increases due to the scattering effect from the gradual formation of aggregates/particles in the solution. It should be noted that the scattering effect usually leads to a fluctuation of fluorescence intensity, which may result in poor stability of the sensing approaches. Fortunately, here we can detect Al^{3+} in a ratiometric manner that can greatly remove this adverse effect.

In order to gain insight into the sensing mechanism of our protocol, we first investigated the pH effect on the binding ability of **3** to Al^{3+}. As mentioned above, the dansylamide fluorophore is sensitive to pH change. Protonation on the dimethylamino group inhibits intramolecular charge transfer and decreases its emission intensity. However, no wavelength shift for the ICT band is observed in the tested pH range (4–9) and

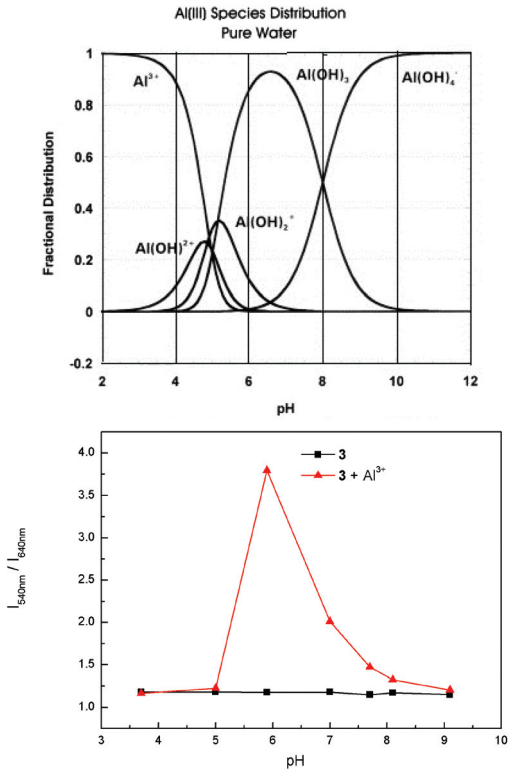

Fig. 5 (Top) Al(III) species distribution as a function of pH in pure water, cited from ref. 32; (bottom) the pH effect on the change of fluorescence intensity at 533 nm of **3** before and after addition of Al^{3+} in lutidine solution (10 mM), λ_{ex} = 328 nm; [**3**] = 10 μM and the pH effect of species of Al^{3+} in pure water. Reprinted with permission from Elsevier. This article was published in Coordination Chemistry Reviews, 228, K. M. Elkins and D. J. Nelson, Spectroscopic approaches to the study of the interaction of aluminium with humic substances, 205–225, Copyright © Elsevier (2002).

thus the ratio of fluorescence intensity at 540 nm and 640 nm remains constant under different pH conditions, as shown in Fig. 5. In the presence of Al^{3+}, the ratio of the resulting complex shows a maximum at pH 6 and decreases dramatically when the pH deviates from 6 (Fig. 5). When the pH is lower than 5 or higher than 8, the addition of Al^{3+} shows almost no influence on the ratio. It is well known that the existing forms of aluminum depend strongly on pH, as shown in Fig. 5 (top).[32] In pure water, when the pH is lower than 4, more than 90% of aluminum exists as free $[Al(H_2O)_6]^{3+}$; with the increase of pH but lower than 7, aluminum hydrolyzes to produce the precipitate $Al(OH)_3$; and when the pH is higher than 7, $Al(OH)_3$ is again transferred into $Al(OH)_4^-$. The pH effect on the spectral response of **3** to Al^{3+} is quite similar to the curve of fraction distribution of $Al(OH)_3$ in water under different pH conditions, though with a narrower half-peak width. It is supposed that **3** with four negative charges can be adsorbed through electrostatic interaction onto the $Al(OH)_3$ colloid surface covered with positive charge. The electrostatic interaction was verified by the reference compound **2**. Under identical conditions in EtOH–lutidine buffer (9 : 1, pH 6.0) (Fig. 6), blue shift and fluorescence enhancement are observed for **3** while they do not occur on **2**.

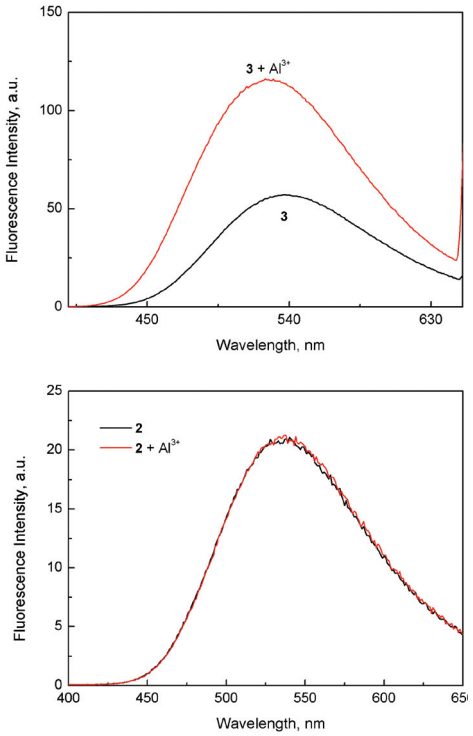

Fig. 6 Fluorescence spectra of **3** (top) and **2** (bottom) in the absence and presence of Al^{3+} in EtOH and lutidine buffer solution (pH = 6.0, 10 mM) mixed solution ($v_{EtOH} : v_{lutidine}$ = 9 : 1); [**2**] = [**3**] = 10 μM, [Al^{3+}] = 0.1 mM, λ_{ex} = 328 nm for **3** and λ_{ex} = 338 nm for **2**.

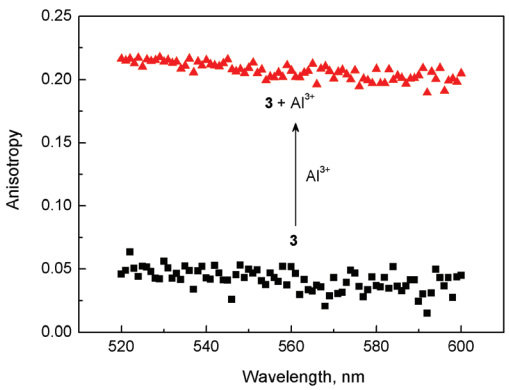

Fig. 7 Anisotropy of **3** in the absence and presence of Al^{3+} in lutidine buffer solution (pH = 6.0, 10 mM); [**3**] = 10 μM, [Al^{3+}] = 0.1 mM, λ_{ex} = 328 nm.

Fluorescence anisotropy measurement is a powerful approach to study the aggregation phenomenon. As can be seen from Fig. 7, free ligand **3** shows a very small anisotropy with the average value of 0.05, which is due to the rapid rotation of the fluorophore on its lifetime scale. It is quite surprising to find that with the addition of 10 equiv. of Al^{3+}, the anisotropy value of the resulting complex was increased to 0.23, as shown in Fig. 7. The significant increase of the anisotropy strongly demonstrates that free ligand **3** is adsorbed onto large particles, which results in a decrease of the rotational diffusion rate. The decrease of the micro-environ-

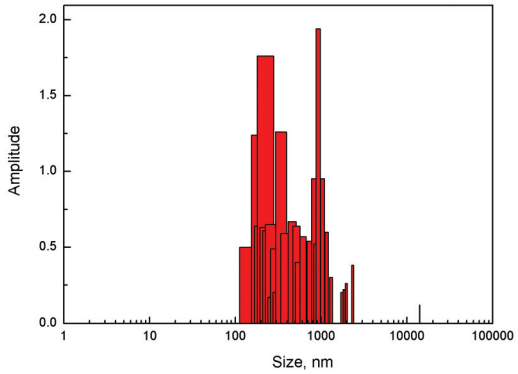

Fig. 8 Dynamic light scattering of **3** in the presence of Al^{3+} in lutidine buffer solution (pH = 6.0, 10 mM); [**3**] = 10 μM, [Al^{3+}] = 0.12 mM.

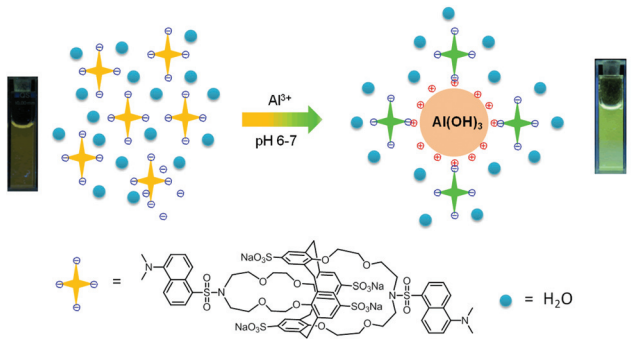

Scheme 2 Schematic illustration of interaction between **3** and Al^{3+}.

mental polarity of the ICT characteristic dansyl fluorophore in the aggregates results in fluorescence enhancement and blue shift. Dynamic light scattering (DLS) was also carried out to confirm the aggregation process. As illustrated by Fig. 8, the polydisperse distribution of particles ranging from hundreds of nm to μm is consistent with our assumption of formation of aggregates between $Al(OH)_3$ and ligand **3** under these conditions. Herein we propose the sensing mechanism for our protocol, as presented in Scheme 2. At the pH 6, formation of $Al(OH)_3$ with positive charge can adsorb negatively-charged **3** to form an aggregate. A reduction of micro-environmental polarity of the ICT characteristic dansyl fluorophore results in fluorescence enhancement and blue shift. And the bulk steric effect resulting from the calix[4]arene moiety prevents formation of compact H-aggregates and retains the high fluorescence quantum yield. These two factors together contribute to the blue shift and fluorescence enhancement.

Selectivity of **3** to Al^{3+} over a wide range of metal ions was then screened in lutidine buffer solution at pH 6.0. As shown in Fig. 9, the addition of very high concentrations of alkali metals Na^+, K^+, Li^+, alkaline earth metals Mg^{2+}, Ca^{2+}, Ba^{2+} at the 10 mM level and transition metal ions Eu^{3+}, La^{3+}, Cd^{2+}, Co^{2+}, Cu^{2+}, Fe^{2+}, Hg^{2+}, Mn^{2+}, Ni^{2+}, Pb^{2+} and Zn^{2+} at 0.1 mM shows almost no effect on the spectral properties of **3**. The addition of Fe^{3+} (0.1 mM), however, decreases the fluorescence intensity without a wavelength shift. In contrast, only the

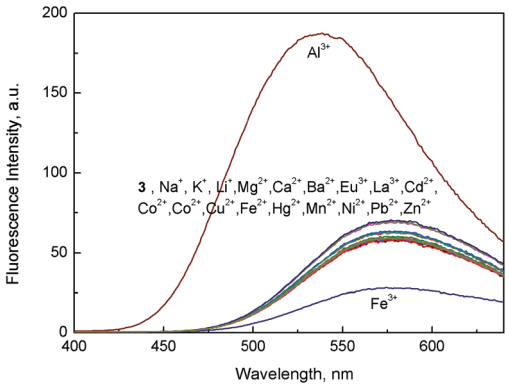

Fig. 9 Absorption and fluorescence spectra of **3** in the presence of various metal ions in lutidine buffer solution (pH = 6.0, 10 mM); [**3**] = 10 μM, alkali and alkaline earth metal ions were 10 mM, and the others were 0.1 mM, λ_{ex} = 328 nm.

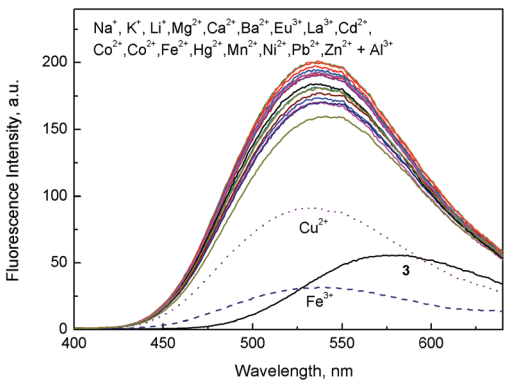

Fig. 10 Fluorescence spectra of **3** in the coexistence of various metal ions and Al^{3+} in lutidine buffer solution (pH = 6.0, 10 mM); [**3**] = 10 μM, alkali and alkaline earth metal ions were 10 mM, and the others were 0.1 mM, λ_{ex} = 328 nm.

addition of Al^{3+} (0.1 mM) induces a remarkable fluorescence enhancement concomitant with a large blue shift from 576 to 530 nm and a fluorescence color change from dark yellow to bright green. Considering the large blue shift of the wavelength with respect to Al^{3+}, selectivity is expressed as the ratio of fluorescence intensity at 540 nm and 640 nm, as shown in Fig. 11. It demonstrates that **3** shows very high selectivity to Al^{3+} over other metal ions. A competition experiment of **3** to Al^{3+} in the presence of other competing metal ions was also carried out. As shown in Fig. 10, all the tested competing ions except Cu^{2+} and Fe^{3+} hardly produced interference in the detection of Al^{3+}. The presence of Cu^{2+} and Fe^{3+} induced fluorescence quenching to different extents; however, they all showed a large blue shift compared with free ligand **3**. When the ratio of fluorescence intensities at 540 nm and 640 nm was used to establish the competition experiment, the interference of Cu^{2+} was eliminated and Fe^{3+} was reduced, as shown in Fig. 11. Therefore **3** was demonstrated to be a promising selective fluorescent chemosensor for aluminum in complex samples.

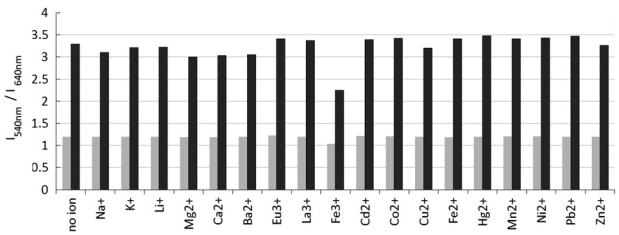

Fig. 11 Ratiometric response I_{540}/I_{640} of **3** in the presence of selected metal ions in lutidine buffer solution (pH = 6.0, 10 mM). The light bars represent the response of **3** in the presence of selected cations; the dense bars represent the response upon an addition of Al^{3+} to a solution of **3** in the presence of selected cations; [**3**] = 10 μM, alkali and alkaline earth metal ions were 10 mM, and the others were 0.1 mM, λ_{ex} = 328 nm.

Conclusions

In conclusion, the new water-soluble fluorescent chemosensor **3** exhibits very high selectivity to Al^{3+} under the weakly acidic condition pH 6.0. Remarkable fluorescence blue shift and about 3-fold enhancement were observed due to the aggregation of **3** on colloidal particles of $Al(OH)_3$, which was verified by the increase of the absorption tail band, pH effect, DLS, anisotropy measurement and also a reference compound **2**. The change of the micro-environmental polarity of the ICT characteristic dansyl fluorophore resulted in fluorescence enhancement and blue shift. The selectivity of our protocol stems from the unique character of the formation of positively-charged $Al(OH)_3$ colloid particles around pH 6.0 and its strong binding affinity with sulfonate. Thus the vast choice of sulfonated chromophore/fluorophores with different ICT characteristics may easily extend our strategy for the selective detection of Al^{3+}.

Experimental section

Materials and methods

Absorption spectra were recorded on a Cary5000 spectrophotometer and corrected emission spectra were performed on Jobin-Yvon Spex Fluorolog 1681 or FluoroMax4 spectrofluorometers (1 cm quartz cell was used). A stock solution (1.0 mM) of compound **3** was prepared in H_2O. Stock solutions of metal nitrate/perchlorate salts were prepared in H_2O.

The tested metal salts included $Al(NO_3)_3{\cdot}9H_2O$, NaSCN, KSCN, $LiClO_4$, $Mg(ClO_4)_2$, $Ca(ClO_4)_2{\cdot}4H_2O$, $Ba(ClO_4)_2$, $FeCl_3{\cdot}6H_2O$, $Eu(NO_3)_3{\cdot}6H_2O$, $La(NO_3)_3{\cdot}4H_2O$, $Cd(ClO_4)_2{\cdot}H_2O$, $Co(ClO_4)_2{\cdot}6H_2O$, $Cu(ClO_4)_2{\cdot}6H_2O$, $Fe(ClO_4)_2{\cdot}xH_2O$, $Hg(ClO_4)_2{\cdot}6H_2O$ $Mn(ClO_4)_2{\cdot}6H_2O$, $Ni(ClO_4)_2{\cdot}6H_2O$, $Pb(ClO_4)_2{\cdot}H_2O$, and $Zn(ClO_4)_2{\cdot}6H_2O$.

Synthesis of ligands

2: Dansylamide (0.114 g, 0.46 mmol) and K_2CO_3 (0.16 g, 1.15 mmol) in dry MeCN (20 mL) were stirred at room temperature for 30 min followed by the addition of compound **1** (0.32 g, 0.23 mmol in MeCN (10 mL)) at one port. The resulting mixture was refluxed overnight. Then the solvent was evaporated and the residue was dissolved in $CHCl_3$, and washed with H_2O twice. The organic layer was dried over $MgSO_4$ and evaporated to obtain the crude product. It was purified by column chromatography over silica (elute: DCM–MeOH (99 : 1)) to obtain the pure product (0.25 g, 47%). ^{1}H NMR (400 MHz, $CDCl_3$): δ 8.54 (d, J = 8.2 Hz, 2H), 8.33 (d, J = 8.7 Hz, 2H), 8.18 (dd, J = 7.3, 1.4 Hz, 2H), 7.59 (t, J = 7.8 Hz, 2H), 7.53 (t, J = 7.4 Hz, 2H), 7.20 (d, J = 7.8 Hz, 2H), 7.04 (d, J = 7.3 Hz, 8H), 6.79 (t, J = 7.4 Hz, 4H), 3.82 (s, 8H), 3.47 (m, 16H), 3.40 (t, J = 5.0 Hz, 8H), 3.04 (t, J = 5.0 Hz, 8H), 2.89 (s, 12H); ^{13}C NMR (100 MHz, $CDCl_3$): 157.3, 151.8, 135.3, 133.6, 130.3, 130.2, 130.1, 129.7, 129.3, 128.1, 123.2, 122.5, 119.7, 115.3, 70.8, 70.3, 69.5, 47.5, 45.5, 38.2 ppm; HRMS (ESI) m/z calcd for $C_{68}H_{76}N_4NaO_{12}S_2$ [M + Na^+] 1227.4799, found 1227.4822.

3: To a solution of compound **2** (110 mg, 0.091 mmol) in dry DCM (3 mL) was added HSO_3Cl (120 μL in 3 mL DCM) dropwise at −20 °C. After stirring at room temperature for 3 h, the solution was poured into ice-water solution and the pH was adjusted to 7 with $NaHCO_3$. The aqueous solution was evaporated to dryness and redissolved in pyridine (6 mL) and water (2 mL). After stirring at room temperature for 2 h, the solution was concentrated (about 1.0 mL). A large precipitate was obtained by the addition of acetone. The precipitate was again dispersed in 0.5 mL H_2O at 30 °C. The insoluble residue was filtered off and washed with acetone to obtain the pure product (80 mg, 54%). ^{1}H NMR (400 MHz, D_2O): δ 8.34 (d, J = 8.7 Hz, 2H), 8.10 (d, J = 7.4 Hz, 2H), 8.06 (d, J = 8.7 Hz, 2H), 7.63 (t, J = 8.2 Hz, 2H), 7.58 (t, J = 7.8 Hz, 2H), 7.43 (s, 8H), 7.28 (d, J = 7.8 Hz, 2H), 3.90 (s, 8H), 3.39 (m, 16H), 3.14 (t, J = 5.0 Hz, 8H), 2.81 (t, J = 5.0 Hz, 8H), 2.73 (s, 12H); ^{13}C NMR (100 MHz, $CDCl_3$): 159.2, 150.4, 137.5, 133.8, 130.0, 129.4, 129.1, 128.9, 126.6, 124.2, 123.2, 119.8, 116.1, 70.0, 68.6, 46.4, 45.0, 36.9 ppm; HRMS (ESI) m/z calcd for $C_{68}H_{72}N_4Na_3O_{24}S_6$ [M − Na^+] 1589.2554, found 1589.2628.

Notes and references

1 S. A. Jenekhe and J. A. Osaheni, *Science*, 1994, **265**, 765–768.
2 Y. Hong, J. W. Lam and B. Z. Tang, *Chem. Commun.*, 2009, 4332–4353.
3 Y. Hong, J. W. Lam and B. Z. Tang, *Chem. Soc. Rev.*, 2011, **40**, 5361–5388.
4 Ü. Ocak, M. Ocak and R. A. Bartsch, *Inorg. Chim. Acta*, 2012, **381**, 44–57.
5 T. Sanjoy Singh and S. Mitra, *J. Lumin.*, 2007, **127**, 508–514.
6 M. Kawahara, K. Muramoto, K. Kobayashi, H. Mori and Y. Kuroda, *Biochem. Biophys. Res. Commun.*, 1994, **198**, 531–535.
7 S. R. Paik, J. H. Lee, D. H. Kim, C. S. Chang and J. Kim, *Arch. Biochem. Biophys.*, 1997, **344**, 325–334.
8 P. F. Good, C. W. Olanow and D. P. Perl, *Brain Res.*, 1992, **593**, 343–346.

9 V. B. Gupta, S. Anitha, M. L. Hegde, L. Zecca, R. M. Garruto, R. Ravid, S. K. Shankar, R. Stein, P. Shanmugavelu and K. S. Jagannatha Rao, *Cell Mol. Life Sci.*, 2005, **62**, 143–158.

10 B. Valeur and I. Leray, *Coord. Chem. Rev.*, 2000, **205**, 3–40.

11 A. P. de Silva, H. Q. N. Gunaratne, T. Gunnlaugsson, A. J. M. Huxley, C. P. McCoy, J. T. Rademacher and T. E. Rice, *Chem. Rev.*, 1997, **97**, 1515–1566.

12 I. Leray and B. Valeur, *Eur. J. Inorg. Chem.*, 2009, 3525–3535.

13 S. Kim, J. Y. Noh, K. Y. Kim, J. H. Kim, H. K. Kang, S. W. Nam, S. H. Kim, S. Park, C. Kim and J. Kim, *Inorg. Chem.*, 2012, **51**, 3597–3602.

14 K. K. Upadhyay and A. Kumar, *Org. Biomol. Chem.*, 2010, **8**, 4892–4897.

15 D. Maity and T. Govindaraju, *Eur. J. Inorg. Chem.*, 2011, 5479–5485.

16 A. Sahana, A. Banerjee, S. Das, S. Lohar, D. Karak, B. Sarkar, S. K. Mukhopadhyay, A. K. Mukherjee and D. Das, *Org. Biomol. Chem.*, 2011, **9**, 5523–5529.

17 M. Arduini, F. Felluga, F. Mancin, P. Rossi, P. Tecilla, U. Tonellato and N. Valentinuzzib, *Chem. Commun.*, 2003, 1606–1607.

18 T. H. Ma, M. Dong, Y. M. Dong, Y. W. Wang and Y. Peng, *Chem. – Eur. J.*, 2010, **16**, 10313–10318.

19 M. Dong, Y. M. Dong, T. H. Ma, Y. W. Wang and Y. Peng, *Inorg. Chim. Acta*, 2012, **381**, 137–142.

20 Y. Lu, S. S. Huang, Y. Y. Liu, S. He, L. C. Zhao and X. S. Zeng, *Org. Lett.*, 2011, **13**, 5274–5277.

21 S. H. Kim, H. S. Choi, J. Kim, S. J. Lee, D. T. Quang and J. S. Kim, *Org. Lett.*, 2010, **12**, 560–563.

22 D. Maity and T. Govindaraju, *Chem. Commun.*, 2010, **46**, 4499–4501.

23 D. Maity and T. Govindaraju, *Chem. Commun.*, 2012, **48**, 1039–1041.

24 T. Y. Han, X. Feng, B. Tong, J. B. Shi, L. Chen, J. G. Zhi and Y. P. Dong, *Chem. Commun.*, 2012, **48**, 416–418.

25 P. Somasundaran, K. P. Ananthapadmanabhan and M. S. Celik, *Langmuir*, 1988, **4**, 1061–1063.

26 I. Leray, Z. Asfari, J. Vicens and B. Valeur, *J. Chem. Soc., Perkin Trans. 2*, 2002, 1429–1434.

27 R. Metivier, I. Leray and B. Valeur, *Photochem. Photobiol. Sci.*, 2004, **3**, 374–380.

28 J. P. Malval, I. Leray and B. Valeur, *New J. Chem.*, 2005, **29**, 1089–1094.

29 V. Souchon, I. Leray and B. Valeur, *Chem. Commun.*, 2006, 4224–4226.

30 S. K. Kim, W. Sim, J. Vicens and J. S. Kim, *Tetrahedron Lett.*, 2003, **44**, 805–809.

31 W. W. H. O. Geneva, *Guidelines for drinking water quality*, 4th edn, 2011.

32 K. M. Elkins and D. J. Nelson, *Coord. Chem. Rev.*, 2002, **228**, 205–225.